An autonomous wearable biosensor powered by a perovskite solar cell

Jihong Min[1,6], Stepan Demchyshyn[2,3,6], Juliane R. Sempionatto[1], Yu Song[1], Bekele Hailegnaw[2,3], Changhao Xu[1], Yiran Yang[1], Samuel Solomon[1], Christoph Putz[2,3], Lukas Lehner[2,3], Julia Felicitas Schwarz[4], Clemens Schwarzinger[4], Markus Scharber[5], Ehsan Shirzaei Sani[1], Martin Kaltenbrunner[2,3]*, Wei Gao[1]*

[1]Andrew and Peggy Cherng Department of Medical Engineering, Division of Engineering and Applied Science, California Institute of Technology, Pasadena, California, 91125, USA.

[2]Division of Soft Matter Physics, Institute of Experimental Physics, Johannes Kepler University Linz, Altenbergerstrasse 69, 4040 Linz, Austria.

[3]Soft Materials Lab, Linz Institute of Technology, Johannes Kepler University Linz, Altenbergerstrasse 69, 4040 Linz, Austria.

[4]Institute for Chemical Technology of Organic Materials, Johannes Kepler University Linz, Altenbergerstrasse 69, 4040 Linz, Austria.

[5]Linz Institute for Organic Solar Cells, Johannes Kepler University Linz, Altenbergerstrasse 69, 4040 Linz, Austria.

[6]These authors contributed equally to this work.

*email: weigao@caltech.edu; martin.kaltenbrunner@jku.at.

Wearable sweat sensors can potentially be used to continuously and non-invasively monitor physicochemical biomarkers that contain information related to disease diagnostics and fitness tracking. However, the development of such autonomous sensors faces a number of challenges including achieving steady sweat extraction for continuous and prolonged monitoring, and addressing the high power demands of multifunctional and complex

analysis. Here we report an autonomous wearable biosensor that is powered by a perovskite solar cell and can provide continuous and non-invasive metabolic monitoring. The device uses a flexible quasi-two-dimensional perovskite solar cell module that provides ample power under outdoor and indoor illumination conditions (power conversion efficiency exceeding 31% under indoor light illumination). We show that the wearable device can continuously collect multimodal physicochemical data — glucose, pH, sodium ions, sweat rate, and skin temperature — across indoor and outdoor physical activities for over 12 hours.

Introduction

The recent shift towards personalized and remote healthcare has accelerated the development and adoption of wearable devices that can continuously monitor physical vital signs as well as biochemical markers[1–15]. Wearable biosensors can potentially be used to continuously and non-invasively analyze body fluids such as sweat, which contains a wealth of information pertinent to disease diagnostics and fitness tracking[1,8,13,16,17]. A variety of electrochemical sensing strategies, including amperometry, potentiometry, voltammetry, and impedance spectroscopy, have been used to detect sweat biomarkers (such as electrolytes, metabolites, nutrients, drugs, and hormones)[1–3,8,17–19] and sweat rate (which may have a close link to secreted biomarker levels)[11,12,20]. For practical health monitoring beyond that during vigorous exercise, wearable biosensors can also benefit from steady sweat extraction via iontophoresis, a localized sedentary sweat stimulation technique[21,22]. However, due to challenges related to multimodal system miniaturization and integration, the development of a wearable system capable of autonomous sweat induction and sampling, real-time sweat rate monitoring, and continuous multiplexed biomarker analysis remains limited.

High power demand also impedes the development of such multifunctional wearable sensing systems. Wearable sensors typically rely on the use of batteries: a bulky and unsustainable power source that requires an external source of electricity to recharge. Various energy harvesting strategies — including biofuel cells and triboelectric nanogenerators — have been explored for powering battery-free wearables[23–29]. However, biofuel cells typically suffer from limited long-term stability due to biofouling in human sweat[23], and triboelectric nanogenerators require extensive physical activity to generate electricity[24]. Furthermore, the power densities produced by biofuel cells and triboelectric nanogenerators from casual daily activities are limited[24,25].

Ambient light, including natural sunlight and artificial indoor light, is an abundant form of energy that is readily available during daily activities. The commercially dominant photovoltaics technologies, which are based on silicon, work well for large-scale solar energy harvesting, but struggle to address the power needs of wearable devices. In particular, silicon cells are often fragile, bulky and rigid. They also provide insufficient power conversion efficiency (PCE) under low or indoor illumination, due to their narrow bandgap and preferentially trap-assisted recombination, limiting their range of applications[30]. Light harvesting technologies based on the III-V family of semiconductors can address some of the limitations of silicon, but their fabrication often requires complex processing conditions, which is reflected in their price/energy payback time and thus their potential areas of application[31,32].

Perovskite solar cells offer a number of favorable intrinsic properties including long charge carrier diffusion lengths, high absorption coefficients, solution processability, small exciton binding energies, high structural defect tolerance, tunable bandgap, and high photoluminescence quantum yields[33,34]. Such solar cells have developed quickly in the last decade due to their evolving

fabrication protocols and the adaptability of the material compositions[35]. Perovskites also offer strong defect tolerance that leads to high parallel resistance (Rp), which is the key parameter of solar cell performance under low light conditions. This results in increased fill factor (FF) and reduced open circuit voltage (Voc) losses at low light conditions, which in combination with the matching of perovskite solar cell spectral response to common indoor lighting emission spectrum, yields high PCE under indoor illumination[30,36].

In this Article, we report an autonomous wearable biosensor that is powered by a flexible perovskite solar cell (FPSC) and can provide continuous and non-invasive metabolic monitoring (**Fig. 1a**). Our multifunctional wearable device offers autonomous sweat extraction via iontophoresis, dynamic microfluidic sweat sampling, multiplexed monitoring of sweat biomarkers using different electrochemical detection techniques, impedance-based sweat rate analysis, and Bluetooth-based wireless data transmission. The wearable device operates under a wide range of illumination conditions ranging from full sunlight to indoor lighting. It is powered by an efficient 2 cm^2 active area lightweight quasi-2D FPSC energy harvesting module with a PCE of 14% under air mass global 1.5 (AM1.5) illumination, and 29.64% under 600 lx indoor illumination with a white light LED light bulb. The sensing platform can be used to continuously collect multimodal physicochemical data (glucose, pH, Na^+, sweat rate, and temperature) across indoor and outdoor physical activities for over 12 hours, and without the need for batteries or vigorous exercise.

Main text

Wearable device design for autonomous biomarker analysis

The wearable device consists of disposable and reusable modules assembled in an origami-like fashion (**Fig. 1b** and **Supplementary Figs. 1,2**). Among the reusable parts is the highly efficient quasi-2D FPSC module that converts ambient light into electrical power and the energy-efficient flexible printed circuit board (FPCB) for electrochemical instrumentation, signal processing, and Bluetooth wireless communication. A daily disposable flexible patch contains a pair of carbachol hydrogel (carbagel) coated iontophoresis electrodes for sweat stimulation, a laser-engraved microfluidic module integrated with interdigitated electrodes for sweat sampling and sweat rate monitoring, and a multiplexed electrochemical sweat biosensor array for molecular analysis (**Fig. 1c**). Compared to traditionally used pilocarpine gels, carbachol gels were selected for iontophoresis as they allow for efficient and long-lasting sudomotor axon reflex sweat secretion from the surrounding sweat glands, ideally suitable for microfluidic sweat sampling[21]. Inkjet printing was used to fabricate all flexible biosensing electrodes and interconnects at a large scale and low cost. Considering that chemical sensors usually suffer from signal drift during long-term use, their capacity for mass-production allows disposable use on a daily or multi-day basis for reliable wearable health monitoring. Potentiometric, amperometric, voltammetric, and impedimetric techniques can all be performed using the wearable device to analyze a broad spectrum of sweat biomarkers ranging from metabolites, electrolytes, nutrients, to substances and drugs. The fully assembled wearable device is 20 mm × 27 mm × 4 mm in size and can comfortably adhere to the skin (**Fig. 1d,e**). The custom embedded algorithm and mobile application enable an energy-saving adaptive power consumption scheme such that the wearable device can extract and analyze sweat across various activities and illumination conditions in a prolonged and efficient

fashion. All calibrated biomarker information can be wirelessly transmitted and displayed on a custom mobile app (**Fig. 1e**, **Supplementary Fig. 3, Supplementary Video 1**).

FPSC design and characterization for wearable use

To effectively and sustainably power the wearable device, an FPSC module (**Fig. 2a**) is designed to have a high power density and PCE for energy harvesting under diverse lighting conditions, flexibility to endure the mechanical stresses common for on-body wear, and stable performance with reliable encapsulation against sweat exposure. The FPSC device utilizes a p-i-n architecture and comprises of flexible polyethylene terephthalate (PET) coated with indium tin oxide (ITO), Cr/Au busbars, a poly(3,4-ethylenedioxythiophene)-poly(styrenesulfonate)(PEDOT:PSS) hole transport layer, quasi-2D perovskite photoactive layer, [6,6]−phenyl-C61-butyric acid methyl-ester (PCBM) electron transport layer, TiO_x interlayer, Cr/Au contacts, and an epoxy/PVC/PCTFE encapsulation (**Fig. 2b**). The perovskite absorber layer (ca. 450 nm thick) with an empirical formula of $(MBA)_2(Cs_{0.12}MA_{0.88})_6Pb_7(I_xCl_{1-x})_{22}$ is at the heart of the device (**Fig. 2c**). A large organic spacer, α-methylbenzylamine (MBA), facilitates the formation of a quasi-2D perovskite structure with large grain size and improved defect passivation, resulting in an excellent device performance (**Supplementary Fig. 4**). Under simulated solar illumination (AM1.5) quasi-2D FPSC with a small active area (0.165 cm^2) achieve PCE of up to 18.1 %, which remains as high as 16.5 % for large area device (1 cm^2), and 14.0% for modules consisting of two large cells joined in series (total active area 2 cm^2) (**Supplementary Fig. 5, Supplementary Table 1**).

The main advantage of our quasi-2D FPSC energy harvesting module is its ability to operate at high efficiency even under indoor and low light illumination conditions. Common indoor lighting sources, like LEDs, have a narrower emission spectrum that closely matches the external quantum

efficiency (EQE) of our quasi-2D FPSC, and a lower photon flux density, when compared to sunlight (**Fig. 2d**). This results in an increased PCE due to reduced sub-bandgap relaxation and recombination losses, as well as passivation of trap states and grain boundaries via MBA incorporation. Thus, quasi-2D FPSC practically double their efficiency under 600 lx (215 μW cm^{-2}) LED indoor illumination, achieving a PCE as high as 31.2 % in small area devices, scaling up efficiently to large area with a PCE of up to 29.9 %, and reaching 29.6 % in module configuration (**Fig. 2e, Supplementary Table 2**). These are the highest reported PCE values among indoor flexible solar cells, outperforming not only perovskite but also other PV technologies in this field (**Supplementary Table 3**). Furthermore, the power output of the quasi-2D FPSC module reliably extends over a broad range of indoor illuminance ranging from very bright (10k lx), common for special environments like surgery rooms, down to dimly lit surroundings (20 lx) (**Fig. 2f, Supplementary Figs. 6** and **7**).

In order to acquire light-source-independent performance values, we also measured PCE using a monochromatic light source (continuous laser, λ = 637 nm) over a range of indoor and low light irradiances ($0.07 < P_{in} < 18$ mW cm^{-2}) (**Supplementary Fig. 8**). We achieved a record breaking PCE of 41.4±0.1% measured at P_{in} = 12.23 mW cm^{-2} for the small area devices, and a PCE of 30.4±0.2% at P_{in} = 6.08 mW cm^{-2} for large area devices (**Supplementary Table 4, Supplementary Note 1**).

The quasi-2D FPSC modules show steady power output with no loss in performance after continuous 24 hours operation under both AM1.5 and indoor illumination conditions (**Fig. 2g, Supplementary Fig. 9**). Additionally, the module mechanical stability was confirmed to withstand

2000 bending cycles (bending radius 5 cm) with only negligible reduction in performance that can be attributed to decrease in ITO electrode resistance (**Fig. 2h, Supplementary Figs. 10** and **11**).

Considering the concern of possible Pb leakage while using perovskite solar cells, a set of Pb-release tests were performed in deionized water (**Supplementary Fig. 12**), as well as in a standard synthetic sweat solution[39,40] on a fully-encapsulated quasi-2D FPSC module (**Fig. 2i**). Continuous operation of the FPSC module under AM1.5 for 24 hours while fully immersed in simulated sweat solution resulted in a Pb concentration that remained more than one order of magnitude below the maximum allowable level in drinking water as per the Joint Food and Agriculture Organization/World Health Organization (FAO/WHO) Expert Committee on Food Additives (JECFA)[41] (**Fig. 2i**), indicating the encapsulation robustness and module safety even under conditions that far exceed the expected operational conditions of the wearable device. Furthermore, the encapsulated FPSC maintained high biocompatibility even after vigorous mechanical bending tests as evidenced by low Pb-leakage as well as high cell viability and metabolic activity of the cells seeded on the FPSCs (**Supplementary Figs. 13** and **14**).

System-level integration and operation of wearable device

Composed of off-the-shelf electronic components, the judiciously designed wearable electrochemical instrumentation system of the wearable device is more powerful in functionality and power-efficient than any other reported wearable sweat analyzer. The battery-free electronic system interfaces with the skin via an inkjet-printed disposable sweat patch that contains two gel-loaded iontophoretic electrodes, three electrochemical sweat biosensors, and one sweat rate sensor embedded in the microfluidics (**Fig. 3a**). The system performs constant-current iontophoresis for sweat induction; amperometry, potentiometry, and voltammetry for continuous analysis of a

variety of sweat biomolecular markers; impedance measurements for sweat rate monitoring; and Bluetooth data communication with the user interface (**Fig. 3b,c**, **Supplementary Figs. 15 and 16**).

More specifically, the wearable device's electronic system consist of: 1) an energy harvesting power management integrated circuit (PMIC) that efficiently boost converts and manages the output from the quasi-2D FPSC, 2) a compact programmable system-on-chip (PSoC) Bluetooth low energy (BLE) module that integrates a microcontroller (MCU) and BLE radio, 3) an electrochemical analog front-end (AFE) that integrates various configurable blocks necessary for electrochemical detection, and 4) a high compliance-voltage current source with an overcurrent protection switch for iontophoresis (**Fig. 3b** and **Supplementary Fig. 17a,b**). Under illumination, the PMIC charges the 5 mF solar energy storage capacitor up to ~5 V to continuously power the wearable device. Our custom-developed embedded algorithm ensures that each block of the system operates at its lowest viable power mode, enabling ultra-low-power multiplexed electrochemical measurements consuming below 60 μW (**Supplementary Fig. 17c** and **Supplementary Fig. 17**). During operation, the wearable device stays in deep-sleep (33 μW during standby) or sleep (47 μW during potentiostat operations) modes and wakes up intermittently to either wirelessly communicate with the host software, perform an electrochemical measurement, or process measurement data (**Supplementary Fig. 19**). Depending on the illumination conditions and the quasi-2D FPSC's power output, the wearable device adapts its operation mode (e.g., parameters such as BLE communication interval and sensor data acquisition interval to mediate power consumption) (**Supplementary Note 2**). The power consumption profiles for each electrochemical operation and the corresponding capacitor charging/discharging curves of the solar energy storage

capacitor when powered by a quasi-2D FPSC module under various illumination conditions (2k–18k lx) are highlighted in **Fig. 3d** as well as **Supplementary Fig. 20** and **Supplementary Table 5**. The electrochemical instrumentation performance of the wearable device was successfully validated by comparing its potentiometric, amperometric, and voltammetric responses to those of a commercial potentiostat (**Supplementary Fig. 21**).

Characterization of device for multimodal biosensing

An iontophoretic sweat induction microfluidic module was carefully designed and optimized for minimal power consumption and prolonged use. Unlike standard pilocarpine gels that can only stimulate local sweat glands directly beneath the agonist gel for a short duration and lead to low sensing accuracy due to the mixing of sweat and gel fluid[15,16], carbagels stimulate local and neighboring sweat glands steadily for extended durations[21,22]. This property enables the use of miniaturized carbagels for prolonged sweat induction and microfluidic neighboring sweat collection on a single patch design. The dimensions and layout of the carbagels with respect to the sweat accumulation reservoir were optimized for minimal size, applied current, and maximal sweat extraction efficiency (**Supplementary Note 3**). The reusable carbagel, capable of stimulating sweat continuously throughout the day, is a part of the mass-producible and disposable microfluidic sensor patch that can be replaced for daily use. To demonstrate the device's wearable use, the sweat processing system was paired with a sensor array consisting of an amperometric enzymatic glucose sensor, potentiometric ion-selective pH and Na^+ sensors, and an impedimetric sweat rate sensor. The individual current, potential, and admittance responses of each sensor were recorded by the wearable device under physiologically relevant target analyte concentrations and/or sweat rates (**Fig. 3e, Supplementary Fig. 22**); linear responses were observed between the

measured electrochemical signals and target concentrations (for glucose sensor), logarithm target concentrations (for pH and Na^+ sensors), and reciprocal flow rate (for sweat rate sensor). While sweat Na^+ and pH levels can individually serve as a potent biomarker for various health conditions, they could synergistically aid in calibrating the sweat rate and glucose sensors, respectively (**Supplementary Fig. 23**). In addition, temperature information recorded by the built-in temperature sensor in the AFE of the wearable device aids in more accurate sensor calibrations during wearable use (**Supplementary Fig. 24**). Moreover, the sweat rate sensor can be reconfigured with different volumetric capacities for desired operation duration (**Supplementary Fig. 25**).

When powered by the quasi-2D FPSC module, the wearable device performs multiplexed on-body measurement sequences under a wide range of indoor illumination conditions. With indoor LED illumination with a brightness as low as 1k lx, the wearable device simultaneously monitors glucose, pH, Na^+, and temperature, along with the periodic impedimetric measurement of sweat rate; when less light as low as 400 lx is available, the wearable device's custom algorithm adapts to decrease the multiplexed measurement frequency and transmits data over BLE advertisements (**Fig. 3f**). With a larger area wearable solar cell (8.9 cm x 7.4 cm), the wearable device performs the same multiplexed on-body measurement sequences under even darker illumination conditions (100-300 lx) (**Supplementary Fig. 26**).

In vitro multimodal analysis of glucose, pH, Na^+, temperature, and flow rate through the assembled microfluidic sensor patch was performed in a phosphate-buffered saline (PBS) solution containing 100 μM glucose under varying flow rates (0.12–3 μL min^{-1}) and under lab-light illumination (1200 lx) (**Fig. 3g**). The glucose, pH, and Na^+ biosensors maintained stable and accurate responses even

at a flow rate as low as 0.12 μL min^{-1}, while the sweat rate sensor responded accurately according to the increasing volume. This indicates that while the integrated biosensors will respond to physiologically-induced analyte level changes during the on-body tests, their performance will not be substantially affected by changes in sweat rates. The long-term stability of the wearable device for continuous energy harvesting and multiplexed biosensing was further validated in a long-term study with a constant flow rate of 1 μL min^{-1} for 100 min under varying indoor illumination conditions (**Supplementary Fig. 27**).

On-body device evaluation for multimodal sweat monitoring

The compact design of the wearable device enables the comfortable and strong adhesion of the device to different body parts with access to ambient light (**Fig. 4a**). When worn on body under various outdoor and indoor illumination conditions, the wearable device harvests energy sufficient to enable iontophoresis and multiplexed sweat biosensing sequences; additionally, the light-powered iontophoresis results in efficient and prolonged sweat extraction to allow dynamic sweat biomarker analysis (**Fig. 4b**, **Supplementary Fig. 28**, and **Supplementary Video 2**). The accuracy of the device's interdigitated electrode-enabled sweat rate sensor during wearable use was successfully validated with image-based colorimetric sweat rate analysis (enabled by filling a color dye in the microfluidic sweat inlet before the on-body test) (**Supplementary Fig. 29a**). Autonomous periodical sweat induction allows prolonged continuous sweat extraction: our pilot studies show that a single sweat induction event was on average able to extract ~52 μL over a duration of 3 hours, while sustaining a steady sweat rate over 0.1 μL min^{-1} (**Supplementary Fig. 29b,c**).

The wearable device's efficient light energy harvesting capability and powerful sweat processing system enable continuous and non-invasive physiochemical monitoring under laboratory illumination conditions. The evaluation of the wearable device for cardiometabolic monitoring was performed by continuously monitoring sweat glucose, pH, Na^+, and sweat rate levels along with the skin temperature of human subjects in both sedentary and exercise trials (**Fig. 4c–f** and **Supplementary Figs. 30 and 31**). In the sedentary studies, light-powered iontophoretic sweat extraction was followed by the continuous monitoring of key biomarkers. In the fasting studies, sweat glucose, pH, Na^+, and skin temperature remained stable while sweat rate rapidly increased in the first 30 min and then gradually decreased (**Fig. 4c**). In the oral glucose intake studies, a substantial increase in sweat glucose was observed through the first hour (**Fig. 4d**). Sedentary fasting and glucose intake studies were repeated twice for two additional subjects (**Supplementary Figs. 30** and **31**). From the sedentary oral glucose intake studies performed across 3 subjects, a high correlation was observed between blood glucose levels and sweat glucose levels (**Supplementary Fig. 32**). Similarly, in the exercise studies, sweat glucose remained relatively stable or slightly decreased during fasting, while clearly elevated glucose levels were observed after oral glucose intake followed by a quick decrease after 30 min (**Fig. 4e,f**). We also noticed a conspicuous discrepancy between pH levels of carbachol iontophoresis-induced sweat (~pH 9) and exercise-induced sweat (~pH 5), indicating the importance of sweat induction approaches and pH calibrations on personalized metabolic monitoring (**Supplementary Fig. 33**). In all sedentary and exercise studies, positive correlations between the real-time calibrated sweat glucose and blood glucose levels were obtained, indicating the high potential of realizing non-invasive glucose monitoring using the wearable device. Potential noise due to motion artifacts during on-body

sensing was mitigated by tightly packing and adhering the miniaturized wearable system onto the skin, where electrochemical sensing was performed in a bound microfluidic reservoir to prevent direct skin-sensor contact. Noise was further reduced by hardware filters integrated on-board as well as smoothing algorithms implemented in the custom app.

Prolonged cross-activity multimodal monitoring of sweat biomarkers in real-life scenarios was enabled by the wearable device as illustrated in **Fig. 4g**. Throughout the day, over a 12-hour time span, the subject performed various physical activities under various lighting environments. During this time, the wearable device performed iontophoresis intermittently to ensure that a sufficient sweat rate could be maintained for sweat refreshing and continuous sensor measurements throughout the day. Depending on the available illumination, the wearable device switched its on-body measurement sequence to adjust its power consumption while trading off for measurement intervals. While the multiplexed data interval varied from 8 s to 60 s throughout the day, the wearable device was able to collect, process, and calibrate sensor data continuously in all scenarios. The glucose trend throughout the day shows that the larger meal during dinner results in a higher and longer sweat glucose spike than the lighter lunch. In addition, the average sweat rate during outdoor sedentary activities was higher than the average sweat rate during indoor sedentary activities while vigorous exercise leads to a substantial increase in sweat rate. Considering that the battery-free version of the wearable device requires access to light for long-term operation, integrating a small battery into the wearable device could realize 24-hour operation (even during sleep) (**Supplementary Figs. 34** and **35**).

Conclusion

We have reported a wearable biosensor platform that is powered by a quasi-2D FPSC. The wearable device can persistently extract sweat and simultaneously monitor physicochemical markers (glucose, pH, Na^+, sweat rate, and skin temperature) via a spectrum of electrochemical techniques (potentiometry, amperometry, voltammetry, and impedimetry). It can achieve this under various illumination conditions (strong outdoor sunlight to dim indoor LED light) and across various activities (sleep to vigorous exercise).

Our quasi-2D FPSC is uniquely suitable for powering wearable technologies. The solar harvesting technology offers high efficiency under indoor and low light illumination conditions, maintains high power conversion efficiency and power output across a wide range of illumination conditions, withstands mechanical stress common for on-body wear during vigorous exercise, and remains safe through proper encapsulation. The wearable solar cell is paired with a compact, wireless, and low-power wearable multichannel electrochemical workstation that dynamically adjusts its power consumption to continuously operate without a battery under varying illumination conditions. The modular design of the wearable device is readily scalable; if required, additional energy harvesting modules can be incorporated.

The microfluidic iontophoretic sweat processing module enables prolonged flow rate-monitored sweat extraction. This allows sweat biosensing to be applied beyond situations where vigorous exercise is required — that is, normal everyday activity — as well as use for patients with mobility impairments. The rate-monitored persistent sweat flow continuously refreshes the sensor reservoir for accurate biomarker measurements; the sensor responses are calibrated in real-time by personalized factors such as skin temperature, sweat pH, and sweat Na^+ to further improve measurement accuracy.

Future work for the technology will involve improving the long-term stability of the sensor patch and investigating the correlation between sweat/blood biomarker levels in large-scale human trials. The wearable device can also be paired with different biosensors based on a wide array of electrochemical detection mechanisms (potentiometry, amperometry, voltammetry, and impedimetry) for the identification of an endless number of target biomarkers. Potential fields of application including sport science and daily tracking, as well care for people with health conditions or impairments.

Methods

Materials and reagents

All chemicals and solvents were purchased from commercial suppliers and used as received, if not stated otherwise.

Agarose, carbachol, potassium chloride (KCl), nickel chloride ($NiCl_2$), potassium (III) ferricyanide ($K_3Fe(Cn)_6$), potassium (IV) ferrocyanide ($K_4Fe(Cn)_6$), glucose oxidase (GOx), glutaraldehyde, bovine serum albumin (BSA), 10X phosphate buffered saline (PBS), 3,4-ethylenedioxythiophene (EDOT), poly(sodium 4-styrenesulfonate) (PSS), sodium ionophore X, bis(2-ethylehexyl) sebacate (DOS), polyvinyl butyral resin BUTVAR B-98 (PVB), polyvinyl chloride (PVC), sodium tetrakis[3,5-bis(trifluoromethyl)phenyl] borate (Na-TFPB), aniline, iron (III) chloride ($FeCl_3$), sodium hydroxide (NaOH), citric acid, ITO covered 125 μm PET foil, lead iodide (PbI_2), lead chloride ($PbCl_2$), methylamine (CH_3NH_2), (R)-(+)-α-methylbenzylamine ($C_8H_9NH_2$), cesium iodide (CsI), hydroiodic acid (HI), N,N-dimethylformamide (DMF), acetylacetone

($CH_3COCH_2COCH_3$), titanium (IV) isopropoxide ($Ti[OCH(CH_3)_2]_4$), 2-methoxyethanol ($CH_3OCH_2CH_2OH$), sodium chloride (NaCl), lactic acid ($C_3H_6O_3$), urea (NH2CONH2), ammonia (NH_4OH), and ethanolamine ($H_2NCH_2CH_2OH$) were purchased from Sigma-Aldrich. Sodium chloride (NaCl), methanol, ethanol, acetone, hydrogen peroxide (30% (w/v)), dextrose (D-glucose) anhydrous, tetrahydrofuran (THF), hydrochloric acid (HCl), tetrachloroauric acid ($HAuCl_4$), and disodium phosphate (Na_2HPO_4) were purchased from Thermo Fisher Scientific. Diethyl ether ($(CH_3CH_2)_2O$), chlorobenzene, hexane, dimethyl sulfoxide (DMSO), PEDOT:PSS aqueous dispersion (Clevios PH1000), and chloroform ($CHCl_3$) were purchased from VWR. [6,6]−phenyl-C61-butyric acid methyl ester (PCBM) was purchased from Solenne BV. Hellmanex III detergent was purchased from Hellma Analytics. Zonyl®FS-300 fluorosurfactant was purchased from Fluka. UV curable flexible epoxy (LP4115) was purchased from DELO Photobond. Liveo Aclar DX 2000 encapsulating polymer (PVC/PCTFE) was purchased from Liveo Research. PDMS (SYLGARD 184) was purchased from Dow Corning. Medical adhesives were purchased from 3M. Polyimide films (12 ~ 75 μm thick) were purchased from DuPont. PET films (12 ~ 250 μm thick) were purchased from McMaster-Carr.

Solar cell fabrication and characterization

Glass substrates (1 × 1 inch, 1 mm thick) were cut and cleaned in an ultrasonic bath for 30 min each in 2 v/v% Hellmanex in DI water solution, 2 × DI water solution, acetone, and isopropanol, and dried using N_2 stream. Flexible ITO-covered PET substrates were patterned using insulating tape for masking and etched using concentrated HCl for 10 min. After that they were also cut to 1 × 1 inch size and washed using the same procedure as for glass. PDMS solution was spin-coated onto glass at 4000 rpm for 30 s and placed on a heat plate at 105 °C for 1 min. After that, flexible

substrates were placed on to the PDMS-covered glass, carefully avoiding any trapped air underneath. Finally, the whole substrate was annealed for 15–20 min at 105 °C. Cr-Au bus bars were deposited via thermal evaporation using a shadow mask (base pressure 3×10^{-6} mbar).

The PEDOT:PSS solution was prepared by mixing Clevios PH1000 stock solution with 7 vol% DMSO and 0.7 vol% Zonyl FS-300. The PEDOT:PSS solution was stirred at room temperature for an hour, then kept at 4 °C overnight. Right after filtering through Minisart RC25 Syringe filter 0.45 µm regenerated cellulose, the PEDOT:PSS solution was spin-coated on the substrates with busbars at 1500 rpm for 45 s (ramp 2 s) followed by 1000 rpm for 2 s (ramp 1 s) and annealed at 120 °C for 15 min. Then the film was washed by spin-coating isopropanol at 1000 rpm for 4 s followed by 4000 rpm for 12 s and annealed again at 120 °C for 15 min.

Perovskite solution ($(MBA)_2(Cs_{0.12}MA_{0.88})_6Pb_7(I_xCl_{1-x})_{22}$) was prepared by mixing PbI_2 (322.4 mg,), $PbCl_2$ (83.5 mg,), (R)-(+)-α-methylbenzylamine iodide (MBAI) (74.7 mg,), and Methylamonium iodide (MAI) (187.7 mg,) in DMF containing 10 vol% acetylacetone and stirred for 1 h at 55 °C. MBAI was synthesized from (R)-(+)-α-methylbenzylamine and hydroiodic acid and purified using diethylether (VWR) and absolute ethanol (Merck Millipore) using a procedure previously described in the literature[42]. MAI was synthesized using an analogous procedure. Afterwards, CsI (~0.12 mmol, from 1.5 M stock solution in DMSO) was added to the mixture and stirred overnight. The solution was filtered using polytetrafluoroethylene (PTFE) syringe filters (0.45 µm; Whatman) before spin-coating. Perovskite solution was then deposited using an anti-solvent procedure inside of the nitrogen (N_2) glovebox. The solution was spin-coated in two steps at 1000 rpm for 5 s with ramp 200 rpm s^{-1} followed by 4000 rpm for 25 s with ramp 2000 rpm s^{-1}.

Approximately ~0.2 mL of chlorobenzene (anti-solvent) was dropped at 15th second for about 3 s. Then the film was annealed at 100 °C for 1 h.

After the film cooled down to room temperature PCBM solution was spin-coated onto the sample at 1500 rpm for 16 s (ramp 2 s) followed by 2000 rpm for 15 s (ramp 2 s). PCBM solution was prepared by dissolving 2 wt% PCBM in chlorobenzene and chloroform (1:1 volume ratio). TiOx solgel was prepared based on procedure reported by Heilgenaw et al[42]. TiO_x was spin-coated at 4000 rpm 30 s (ramp 2 s) and annealed at 110 °C for about 5 min in an ambient atmosphere. Cr/Au contacts were evaporated at rate of 0.01-0.5 nm s^{-1} and base pressure 3×10^{-6} mbar. Finally, the devices were encapsulated using UV curable flexible epoxy and PVC/PCTFE protective films. Absorbance spectra were recorded using LAMBDA 1050 UV/Vis Spectrophotometer, Perkin Elmer, U.S.A. Photoluminescence spectra were recorded on a photomultiplier tube–equipped double-grating input and output fluorometer (Photon Technology International).

Current density-voltage (J-V) characteristics of solar cells under sunlight illumination were recorded under simulated AM1.5 global spectrum irradiation from a 150 W xenon light source using Keithley 2400 source meter and a custom Lab-View program. The intensity of the solar simulator was adjusted using a commercial Si reference diode (Si-01TC, Ingenieurburo Mencke & Tegtmeyer, Germany). The performance of the solar cells under indoor lighting was tested using a set of commercial off-the-shelf warm light LED light bulbs (Philips, 2700 K, 4.3 W, 470 lm; Philips, 2700 K, 7 W, 806 lm; Osram, 2700 K, 21 W, 2451 lm). The measurement was performed inside of a light-tight black cloth-covered characterization chamber with the cell tightly wrapped with black tape, allowing only the active area to be exposed to the light, thus reducing the influence of reflections or stray light. A broad range of intermediate illuminance levels was achieved by

utilizing a set of neutral density filters placed directly on the device. The emission spectrum of the light bulbs was measured using a fiber spectrometer (Avantes, AvaSpec-2048-USB2) (**Supplementary Fig. 6**) Illuminance of the LED light sources was measured using ISO calibrated lux meter (Voltcraft MS-1300). Spectral incident power intensity of the LED light bulbs was calculated as reported in literature[43]. Additionally, reference PCE under low light conditions was calculated from a JV curve measured under a monochromatic light source (637 nm laser, Coherent OBIS 637 nm, 140 mW), with the incident power intensity calculated using a calibrated Si diode (Hamamatsu S2281).

Surface SEM measurements were made using the Zeiss 1540 XB CrossBeam SEM (acceleration voltage 5 keV). A cross-section image was prepared by prepared using a standard focus ion beam cutting approach. Images of the cross-section were performed under the same conditions as surface SEM measurements.

Maximum Power Point (MPP) tracking was performed using an in-house written Python script utilizing a common Perturb-and-Observe algorithm. Starting voltage for the measurements was $V_{oc} \cdot FF$, with a step size of 50 mV and 15 s waiting time between voltage perturbations.

Lead release test was performed using standard artificial sweat solution (containing sodium chloride 0.5 % w/w, lactic acid 0.1 % w/w, and urea 0.1 % w/w in deionized water) as described in European Standard EN 1811:1998. Encapsulated solar cell modules were immersed into 100 mL freshly prepared synthetic sweat buffer and placed at about 20 cm under a xenon lamp solar simulator with AM1.5G spectrum (distance adjusted so to achieve approximately 1 Sun illumination). The buffer was continuously stirred with a magnetic stirrer and 1 mL extract samples were collected periodically and stored in the fridge at 4 °C until the next day when they were

analyzed using inductively coupled plasma mass spectrometry (ICP-MS). Alternatively the lead tests were also performed with just deionized water, following the same procedure described above.

Each ICP-MS sample was extracted with 18.2 MOhm water. The extracts were measured without further dilution on an XSeries 2, Thermo Scientific ICP-MS instrument equipped with a MiraMist nebulizer. Calibration was performed with a Certipur multielement standard XXI.

In vitro cell studies

Normal Adult human dermal fibroblast cells (HDFs, Lonza) were cultured in manufacturer's recommended media (FGMTM-2 Growth Media) under 37 °C and 5% CO2. The cells were then passaged at 80% confluency (passage number 5) and were used for all cell studies. For in vitro cytocompatibility tests, two groups of FPSCs (before and after bending) were placed in media during the course of study to release the possible undesired toxic residuals. The HDF cells were seeded into 24 well plates (1 × 105 cells per well) and were treated with appropriate media and incubated under 37 ºC and 5% CO2 for up to 7 days. For the control, cells were treated with fresh media without contact with FPSCs. Cell viability was evaluated by using a commercial calcein AM/ethidium homodimer-1 live/dead kit (Invitrogen) on day 1 and 7 post culture. The samples were then visualized by using an Axio Observer inverted microscope (ZEISS) and cell viability was calculated using ImageJ software and reported as the ratio of live cells to total number of cells (live + dead). A commercial PrestoBlue assay (Thermo Fisher) was also used to evaluate cell metabolic activity according to manufacturer's protocol.

Electronic system design and characterization

The electronic system consists of four main blocks for power management, data processing and wireless communication, electrochemical instrumentation, and iontophoretic induction (**Supplementary Fig. 8**). The power management block consists of an energy harvesting PMIC (BQ25504, Texas Instruments) and a voltage regulator (ADP162, Analog Devices). The PMIC utilizes maximum point power tracking (MPPT) to efficiently boost charge the solar cell output of 5 V and charge the 5mF energy storage capacitor. The threshold control unit of the PMIC enables the capacitor to power the rest of the system while the capacitor voltage stays within a threshold voltage between 3~5 V. The voltage regulator then regulates the capacitor voltage to a stable 2.8 V to supply the data processing and wireless communication, and electrochemical instrumentation blocks.

Data processing and wireless communication are performed by a compact programmable system-on-chip (PSoC) BLE module (Cyble-222014, Cypress Semiconductor) that integrates a microcontroller (MCU) and BLE radio, and electrochemical instrumentation is performed by an electrochemical front-end (AD5941, Analog Devices) and voltage buffers (MAX40018, Analog Devices) that integrate various configurable blocks necessary for electrochemical detection. The PSoC BLE module communicates with the host software via BLE and controls the Electrochemical AFE via serial peripheral interface (SPI). The electrochemical AFE is the core of the platform. The electrochemical AFE's configurable amplifiers can be configured for various electrochemical measurements at multiple modes of measurement ranges and resolutions. For high bandwidth impedance measurements, the high speed loop can be configured, and for lower bandwidth measurements such as potentiometry, amperometry, and voltammetry, the low-power loop can be configured. The AFE contains multiple elements such as a sequencer, a memory block, a waveform

generator, and a DFT hardware accelerator that enables independent operation of complex electrochemical procedures, minimizing the workload of the microcontroller and the overall power consumption. Furthermore, a switch matrix and multiplexer flexibly connect the sensors and analog signals to the appropriate channels.

The iontophoresis induction block generates a high compliance-voltage constant current with current monitoring to safely deliver current across the skin through a gel. A boost converter (TPS61096, Texas Instruments) boosts the energy storage capacitor voltage from the PMIC to a high compliance-voltage, and a BJT array (BCV62C, Nexperia) is configured as a current mirror to supply a steady current through the analog switch (DG468, Vishay Intertechnology) while the iontophoresis block is actuated. Furthermore, the electrochemical AFE's switch matrix enables the iontophoresis block to flexibly connect to the electrochemical AFE's low-power current measurement channel for iontophoresis current monitoring overcurrent protection during iontophoresis.

The wearable device was powered by a custom developed quasi-2D FPSC in most experiments, The power consumption of the system was characterized using a power profiler (PPK2, Nordic Semiconductor), and the energy storage capacitor charging-discharging curves were collected using an electrochemical workstation (CHI 660E). For experiments under bright to room-light illumination conditions (>400 lx), a custom developed quasi-2D FPSC was used to power the wearable device; for experiments under dim-light illumination conditions (<300 lx), a commercial flexible solar cell was used (LL200-2.4-75, PowerFilm Inc.). To validate the performance of the wearable device for electrochemical measurements, we compared the potentiometric,

amperometric, and voltammetric responses collected by the wearable device under laboratory-light mode with those collected by an electrochemical workstation (CHI 660E).

Microfluidic sensor patch fabrication and assembly

The PI substrates were cleaned prior to inkjet printing via O_2 plasma surface treatment (Plasma Etch PE-25, 10–20 cm^3 min^{-1} O_2, 100 W, 150–200 mTorr) to remove debris and improve surface hydrophilicity. Next, an inkjet printer (DMP-2850, Fujifilm) was used for the sequential printing of silver (interconnects and connection pads, interdigitated sweat rate sensor, and reference electrode), carbon (iontophoresis, counter, and working electrodes), and PI (encapsulation). The reference and working electrodes were further modified via electrochemical deposition (CHI 660E) and drop-casting methods for selective electrochemical sensing. Meanwhile, a 50 W CO_2 laser cutter (Universal Laser System) was used to pattern M-tape (3M 468MP) and PET layers to be further assembled onto the sensor patch for microfluidic sweat processing. Z-axis conductive tape (3M 9703) was used to electrically connect the encapsulated PCBs, solar cells, and microfluidic sensor patch through the connection pads and interconnects printed on the PI substrate.

Both anode and cathode carbagels were prepared by heating DI water containing 3% w/w agarose to 250 °C under constant stirring until the mixture became homogenous. After cooling down the mixture to 165 °C, 1% w/w carbachol was added to the anode mixture, and 1% w/w KCl was added to the cathode mixture. Then, the mixtures were poured into the assembled microfluidic sensor patches' carbagel cutouts, where the hydrogels solidified.

Biosensor preparation and characterization

An electrochemical workstation (CHI 660E) was used for electrochemical deposition, and both the electrochemical workstation and the wearable device were used for sensor characterization.

Reference electrode: To form Ag/AgCl, 0.1 M $FeCl_3$ was drop-casted onto the inkjet-printed Ag reference electrode for 30 s. A PVB reference cocktail was prepared by dissolving 79.1 mg of PVB, 50 mg of NaCl, 1 mg of F127, and 0.2 mg of MWCNT into 1 ml of methanol. 1.66 µL of the PVB reference cocktail was drop-casted onto the Ag/AgCl reference electrode and left to dry overnight such that the reference electrode can maintain a steady potential regardless of the ionic strength of the solution.

Glucose sensor: Au nano-dendrites were modified on a carbon working electrode by applying a pulsed voltage from -0.9 V to 0.9 V at a frequency of 50 Hz in a solution containing 50 mM $HAuCl_4$ and 50 mM HCl. A Prussian blue layer was electrochemically deposited on the modified working electrode by performing cyclic voltammetry from -0.2 V to 0.6 V at a scan rate of 50 mV s^{-1} for 20 cycles in a solution containing 2mM $FeCl_3$, 2.5 mM $K_3[Fe(CN)_6]$, 0.1 M KCl, and 0.1 M HCl. Then, the electrode was further modified by performing cyclic voltammetry from 0 V to 0.8 V at a scan rate of 100 mV s^{-1} for 8 cycles in a solution containing 5 mM $NiCl_2$, 2.5 mM $K_3[Fe(CN)_6]$, 0.1 M KCl, and 0.1 M HCl. A GOx enzyme cocktail was prepared by mixing 99 uL of 1% BSA, 1 uL of 2.5 % glutaraldehyde, and 0.25 uL of 10 mg/mL GOx. 1.66 µL of the enzyme cocktail was drop-casted onto the modified working electrode and left overnight to dry.

Sodium sensor: A carbon working electrode was modified in a solution containing 30 mg $K_4[Fe(CN)_6]\cdot 3H_2O$, 206.1 mg NaPSS, 10.7 µL EDOT in 10 mL DI water by applying a constant potential of 0.865 V for 10 min. A Na^+ selective membrane cocktail was prepared by dissolving 1 mg of Na ionophore X, 0.55 mg Na-TFPB, 33 mg PVC, and 65.45 mg DOS into 660 µL THF. 1.66

μL of the Na^+ selective membrane cocktail was drop-casted onto the modified carbon working electrode and left to dry overnight.

pH sensor: Au was deposited on a carbon working electrode by applying a constant potential of 0 V for 30 s in a solution containing 50 mM $HAuCl_4$ and 50 mM HCl. A PANI layer was electropolymerized on the Au modified working electrode by performing cyclic voltammetry from -0.2 V to 1 V at a scan rate of 50 mV s^{-1} for 50 cycles.

Biosensor characterization: For in vitro characterizations for the Na^+ and sweat rate sensors, NaCl solutions (12.5–200 mM) were prepared in DI water. For characterization of the pH sensors, Mcllvaine's buffers with pH values ranging from 4 to 8, and HCl-mediated Mcllvaine's buffer with a pH of 10 were used. For characterization of the glucose sensors, glucose solutions (0–200 μM) were prepared in PBS buffers with pH ranging from 4 to 10. For characterization of the sensors' dependence on temperature, a ceramic hot plate (Thermo Fisher Scientific) was used. For in vitro flow tests, a syringe pump (78-01001, Thermo Fisher Scientific) was used to inject various fluids through the microfluidic sensor patch at flow rates varying form (0.12–3 μL min^{-1}).

On-body evaluation of the wearable device

The validation and evaluation of the wearable device were performed using human subjects in compliance with the ethical regulations under protocols (ID 19-0892 and 21-1079) that were approved by the Institutional Review Board (IRB) at the California Institute of Technology (Caltech). Participating subjects between the ages of 18 and 65 were recruited from the Caltech campus and neighboring communities through advertisement by posted notices, word of mouth, and email distribution. All subjects gave written informed consent before participation in the study.

For all human studies, subjects cleaned their skin with water and alcohol swabs before applying the wearable device on the skin.

System evaluation conditions: For chemical sweat induction, the subjects were illuminated under bright-light conditions for 10 min to enable light-powered iontophoresis (55 μA, 10 min). Following iontophoretic stimulation, the subjects were illuminated under either bright-light (14k lx), laboratory-light (1200 lx), or room-light (600 lx) illumination conditions to enable continuous biomarker detection for the remainder of the study. Sweat rate was measured periodically either with the impedimetric sweat rate sensor, visually, or by both ways.

System evaluation with sugar intake: For fasting and intake studies, subjects reported to the laboratory after fasting overnight. For the iontophoresis-based studies, the wearable device was applied to the ventral forearm region and the subject was illuminated under bright-light (14k lx) conditions for the first 10 minutes to power iontophoresis. For the remainder of the study, the subject was illuminated under lab-light (1200 lx) conditions at rest, while the wearable device performed wireless multimodal monitoring of sweat biomarkers with multiplexed glucose, pH, sodium, and temperature measurements occurring at 8 s intervals, and sweat rate measurements occurring at 5 min intervals. The data was wirelessly transmitted in real-time via BLE indications. For the iontophoresis intake study, the subject was provided a soft drink containing 55 g of sugars. For the exercise-based studies, the wearable device was applied to the forehead region, and the subject was illuminated under lab-light (1200 lx) conditions throughout the entire study, wherein subjects performed constant-load cycling (50 rpm) on a stationary exercise bike (Kettler Axos Cycle M-LA) for 60 minutes. For the exercise intake study, the subject was provided a soft drink containing 55 g of sugars.

System evaluation during daily activities: For the full day study spanning from 9 AM to 9 PM, the subject was iontophoretically stimulated *via* the wearable device for 10 min at 9 AM, 12 PM, 3 PM, and 6 PM. The microfluidics was reset before each iontophoresis section to obtain continuous sweat rate reading. From 9 AM to 1 PM, the subject was outdoors under the sun (100k lx); from 1 PM to 6 PM, the subject was under lab-light (1200 lx) conditions; and from 6 PM to 9 PM, the subject was in room-light (600 lx) conditions. From 9 AM to 6 PM, the wearable device performed multiplexed glucose, pH, Na^+, and temperature measurements occurring at 8 s intervals, and sweat rate measurements occurring at 5 min intervals. The data was wirelessly transmitted *via* BLE indications. From 6 PM to 9 PM, the wearable device performed multiplexed glucose, pH, sodium, and temperature measurements occurring at 60 s intervals and transmitted the data wirelessly *via* BLE advertisements, while sweat rate was evaluated optically every 10 min.

Data availability

The main data supporting the results in this study are available within the paper and its Supplementary Information. Source data for human studies in Figure 4 are provided with this paper. All raw and analyzed datasets generated during the study are available from the corresponding author on request.

Acknowledgements

This project was supported by the National Institutes of Health grants R01HL155815 and R21DK13266, Office of Naval Research grants N00014-21-1-2483 and N00014-21-1-2845, the Translational Research Institute for Space Health through NASA NNX16AO69A, and National Science Foundation grant 2145802, (to W.G.) and by the European Research Council Starting

Grant ‘GEL-SYS’ under grant agreement no. 757931 (to M.K.). S.D. would like to also acknowledge Marshall Plan Foundation that provided financial support for 3 months research visit to California Institute of Technology that initiated this work.

Author contributions

W.G., J.M., M.K., and S.D. initiated the concept and designed the studies; J.M. and S.D. led the experiments and collected the overall data; J.R.S., Y.S., B.H., C.X., Y.Y., and S. S. contributed to wearable device characterization, validation, and sample analysis. B.H., C.P., L.L., M.S., S.S. contributed to solar module development, fabrication, and characterization. S.D., B.H., J.F.S., and C. S. contributed to experimental design and characterization of Pb leakage test for the solar cell module. E.S.S. contributed to cell viability and metabolic activity characterization. J.M., S.D., W.G., and M.K. co-wrote the paper. All authors contributed to the data analysis and provided the feedback on the manuscript.

Competing interests

The authors declare no competing interests.

References

1. Kim, J., Campbell, A. S., de Ávila, B. E.-F. & Wang, J. Wearable biosensors for healthcare monitoring. *Nat. Biotechnol.* **37**, 389–406 (2019).
2. Ray, T. R. *et al.* Bio-integrated wearable systems: A comprehensive review. *Chem. Rev.* **119**, 5461–5533 (2019).
3. Yang, Y. & Gao, W. Wearable and flexible electronics for continuous molecular monitoring. *Chem. Soc. Rev.* **48**, 1465–1491 (2019).

4. Heikenfeld, J. *et al.* Accessing analytes in biofluids for peripheral biochemical monitoring. *Nat. Biotechnol.* **37**, 407–419 (2019).
5. Libanori, A., Chen, G., Zhao, X., Zhou, Y. & Chen, J. Smart textiles for personalized healthcare. *Nat. Electron.* **5**, 142–156 (2022).
6. Someya, T., Bao, Z. & Malliaras, G. G. The rise of plastic bioelectronics. *Nature* **540**, 379–385 (2016).
7. Bariya, M., Nyein, H. Y. Y. & Javey, A. Wearable sweat sensors. *Nat. Electron.* **1**, 160–171 (2018).
8. Gao, W. *et al.* Fully integrated wearable sensor arrays for multiplexed in situ perspiration analysis. *Nature* **529**, 509–514 (2016).
9. Choi, J., Ghaffari, R., Baker, L. B. & Rogers, J. A. Skin-interfaced systems for sweat collection and analytics. *Sci. Adv.* **4**, eaar3921 (2018).
10. Bandodkar, A. J. *et al.* Battery-free, skin-interfaced microfluidic/electronic systems for simultaneous electrochemical, colorimetric, and volumetric analysis of sweat. *Sci. Adv.* **5**, eaav3294 (2019).
11. Nyein, H. Y. Y. *et al.* Regional and correlative sweat analysis using high-throughput microfluidic sensing patches toward decoding sweat. *Sci. Adv.* **5**, eaaw9906 (2019).
12. Kim, S. *et al.* Soft, skin-interfaced microfluidic systems with integrated immunoassays, fluorometric sensors, and impedance measurement capabilities. *Proc. Natl. Acad. Sci. U.S.A.* **117**, 27906–27915 (2020).
13. Son, D. *et al.* Multifunctional wearable devices for diagnosis and therapy of movement disorders. *Nat. Nanotech.* **9**, 397–404 (2014).

14. Niu, S. *et al.* A wireless body area sensor network based on stretchable passive tags. *Nat. Electron.* **2**, 361–368 (2019).
15. Sempionatto, J. R. *et al.* An epidermal patch for the simultaneous monitoring of haemodynamic and metabolic biomarkers. *Nat. Biomed. Eng.* **5**, 737–748 (2021).
16. Emaminejad, S. *et al.* Autonomous sweat extraction and analysis applied to cystic fibrosis and glucose monitoring using a fully integrated wearable platform. *Proc. Natl. Acad. Sci. U.S.A.* **114**, 4625–4630 (2017).
17. Lee, H. *et al.* Wearable/disposable sweat-based glucose monitoring device with multistage transdermal drug delivery module. *Sci. Adv.* **3**, e1601314 (2017).
18. Yang, Y. *et al.* A laser-engraved wearable sensor for sensitive detection of uric acid and tyrosine in sweat. *Nat. Biotechnol.* **38**, 217–224 (2020).
19. Torrente-Rodríguez, R. M. *et al.* Investigation of cortisol dynamics in human sweat using a graphene-based wireless mHealth system. *Matter* **2**, 921–937 (2020).
20. Kwon, K. *et al.* An on-skin platform for wireless monitoring of flow rate, cumulative loss and temperature of sweat in real time. *Nat. Electron.* **4**, 302–312 (2021).
21. Sonner, Z., Wilder, E., Gaillard, T., Kasting, G. & Heikenfeld, J. Integrated sudomotor axon reflex sweat stimulation for continuous sweat analyte analysis with individuals at rest. *Lab Chip* **17**, 2550–2560 (2017).
22. Simmers, P., Li, S. K., Kasting, G. & Heikenfeld, J. Prolonged and localized sweat stimulation by iontophoretic delivery of the slowly-metabolized cholinergic agent carbachol. *J. Dermatol. Sci.* **89**, 40–51 (2018).

23. Yu, Y. *et al.* Biofuel-powered soft electronic skin with multiplexed and wireless sensing for human-machine interfaces. *Sci. Robot.* **5**, eaaz7946 (2020).
24. Song, Y. *et al.* Wireless battery-free wearable sweat sensor powered by human motion. *Sci. Adv.* **6**, eaay9842 (2020).
25. Yin, L. *et al.* A passive perspiration biofuel cell: High energy return on investment. *Joule* **5**, 1888–1904 (2021).
26. Yin, L. *et al.* A self-sustainable wearable multi-modular E-textile bioenergy microgrid system. *Nat. Commun.* **12**, 1542 (2021).
27. Xu, F. *et al.* Scalable fabrication of stretchable and washable textile triboelectric nanogenerators as constant power sources for wearable electronics. *Nano Energy* **88**, 106247 (2021).
28. Park, S. *et al.* Self-powered ultra-flexible electronics via nano-grating-patterned organic photovoltaics. *Nature* **561**, 516–521 (2018).
29. Meng, K. *et al.* A wireless textile-based sensor system for self-powered personalized health care. *Matter* **2**, 896–907 (2020).
30. Polyzoidis, C., Rogdakis, K. & Kymakis, E. Indoor perovskite photovoltaics for the internet of things—challenges and opportunities toward market uptake. *Adv. Energy Mater.* **11**, 2101854 (2021).
31. Mathews, I., King, P. J., Stafford, F. & Frizzell, R. Performance of III–V solar cells as indoor light energy harvesters. *IEEE J. Photovoltaics* **6**, 230–235 (2016).
32. Espinosa, N., Hösel, M., Angmo, D. & Krebs, F. C. Solar cells with one-day energy payback for the factories of the future. *Energy Environ. Sci.* **5**, 5117–5132 (2012).

33. Roy, P., Kumar Sinha, N., Tiwari, S. & Khare, A. A review on perovskite solar cells: Evolution of architecture, fabrication techniques, commercialization issues and status. *Sol. Energy* **198**, 665–688 (2020).
34. Gao, F., Zhao, Y., Zhang, X. & You, J. Recent progresses on defect passivation toward efficient perovskite solar cells. *Adv. Energy Mater.* **10**, 1902650 (2020).
35. Green, M. A. *et al.* Solar cell efficiency tables (Version 58). *Prog. Photovolt. Res. Appl.* **29**, 657–667 (2021).
36. Zheng, H. *et al.* Emerging organic/hybrid photovoltaic cells for indoor applications: Recent advances and perspectives. *Sol. RRL* **5**, 2100042 (2021).
37. Hashemi, S. A., Ramakrishna, S. & Aberle, A. G. Recent progress in flexible–wearable solar cells for self-powered electronic devices. *Energy Environ. Sci.* **13**, 685–743 (2020).
38. Zhao, J. *et al.* A fully integrated and self-powered smartwatch for continuous sweat glucose monitoring. *ACS Sens.* **4**, 1925–1933 (2019).
39. Mallick, A. & Visoly-Fisher, I. Pb in halide perovskites for photovoltaics: reasons for optimism. *Mater. Adv.* **2**, 6125–6135 (2021).
40. Hamann, D. *et al.* Jewellery: alloy composition and release of nickel, cobalt and lead assessed with the EU synthetic sweat method. *Contact Derm.* **73**, 231–238 (2015).
41. World Health Organization. Regional Office for Europe. (2000). Air quality guidelines for Europe, 2nd ed.. World Health Organization. Regional Office for Europe. https://apps.who.int/iris/handle/10665/107335.
42. Hailegnaw, B. *et al.* Inverted (p–i–n) perovskite solar cells using a low temperature processed TiO_x interlayer. *RSC Adv.* **8**, 24836–24846 (2018).

43. Venkateswararao, A., Ho, J. K. W., So, S. K., Liu, S.-W. & Wong, K.-T. Device characteristics and material developments of indoor photovoltaic devices. *Mater. Sci. Eng. R Rep.* **139**, 100517 (2020).

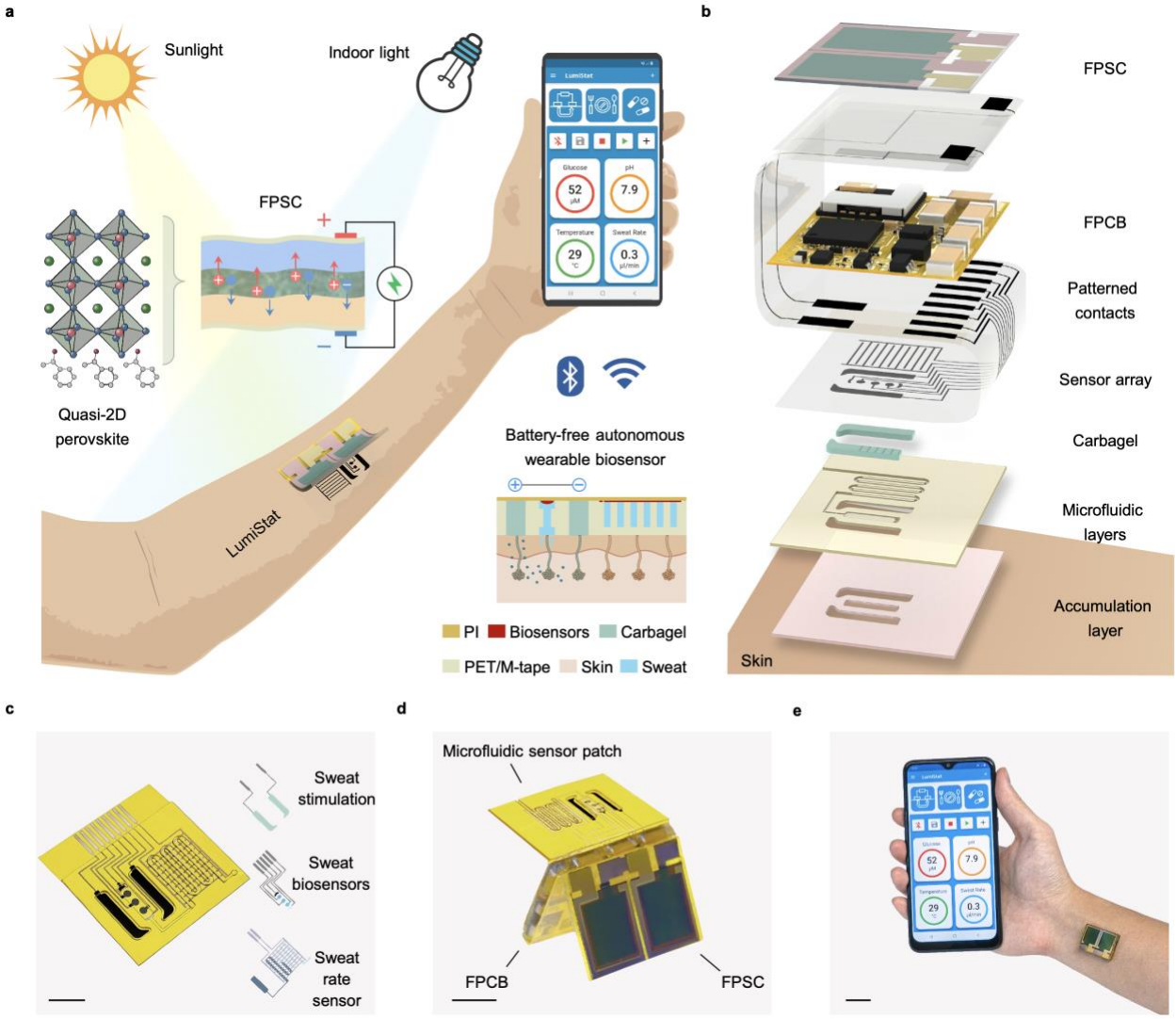

Figure 1 | Schematics and images of the ambient light-powered battery-free lab on the skin. **a**, Illustration of the energy autonomous wearable device that is powered from both outdoor and indoor illumination *via* a quasi-2D flexible perovskite solar cell (FPSC) and perform multiplexed wireless biomolecular analysis across a wide range of activities. Carbagel, carbachol hydrogel; M-tape, medical tape; PET, polyethylene terephthalate; PI, polyimide. **b**, Exploded 3D model of the layer assembly of the wearable device. **c**, Photo of an inkjet-printed disposable microfluidic sensor patch that contains an iontophoretic module for autonomous sweat stimulation, microfluidics for sweat sampling, multiplexed electrochemical biosensors for perspiration analysis, and an impedimetric sweat rate sensor. Scale bar, 0.5 cm. **d**, Photo of the wearable device assembled in origami-style. Scale bar, 1 cm. **e**, Photo of the wearable device worn on the ventral forearm and wirelessly connected to a custom developed mobile app over BLE. Scale bar, 2 cm.

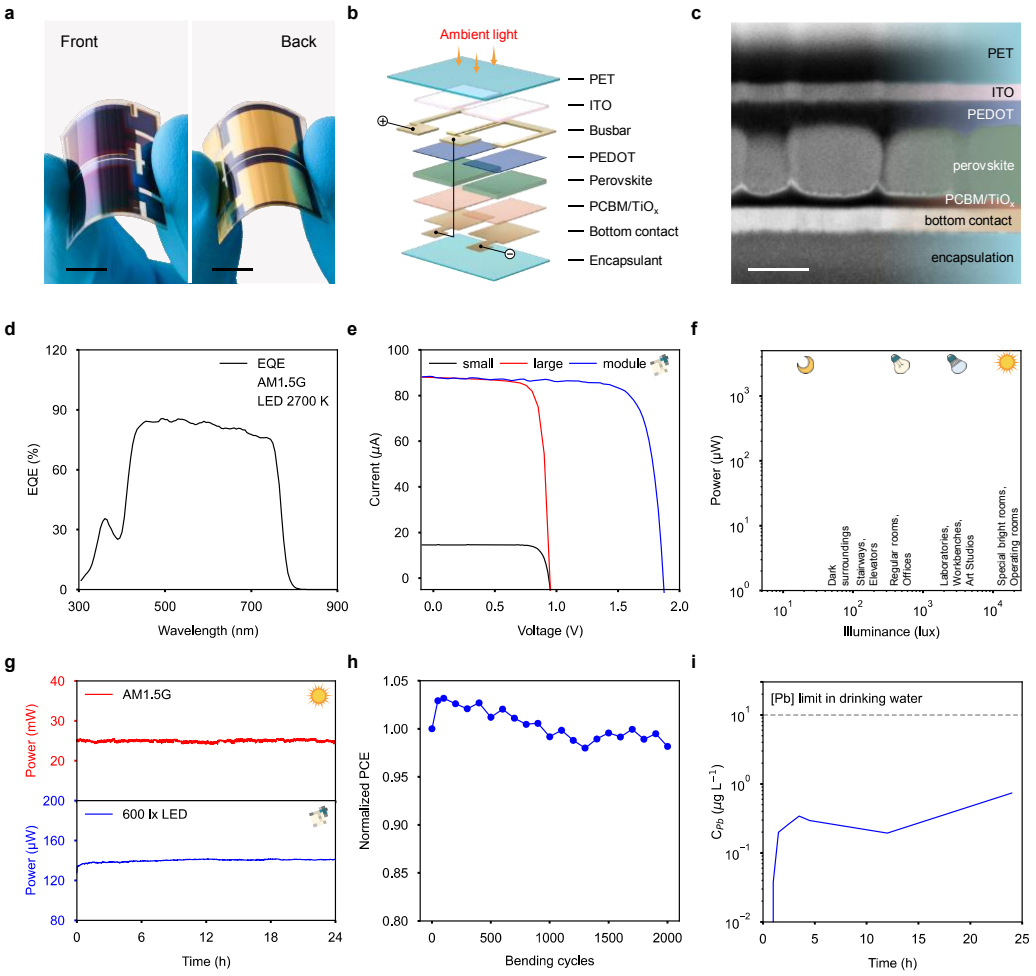

Figure 2 | Design and characterization of the flexible perovskite solar cell. a, Photograph of an FPSC. Scale bar, 1 cm. **b**, 3D model of FPSC module architecture consisting of 2 individual 1 cm^2 active area solar cells connected in series. **c**, Cross-sectional scanning electron microscopy (SEM) image of the FPSC. Scale bar, 400 nm. Experiments were repeated five times independently with similar results. **d**, External quantum efficiency (EQE) of FPSC superimposed with normalized emission spectrum of standard reference AM1.5G tilt sun illumination and room-light (2700 K) LED light bulb spectrum. **e**, IV curves of small (0.165 cm^2), large (1 cm^2), and module (2 cm^2) FPSCs recorded room-light LED light bulb illumination (2700 K, 600 lx). **f,** The power output of a FPSC module as a function of illuminance. R^2, coefficient of determination of the linear regression. **g,** Maximum power point tracking of FPSC module under full sunlight AM1.5G and indoor warm light LED 600 lx illumination over 24 hours. **h**, Normalized PCE of FPSC module as a function of 2000 bending cycles (5 cm bending radius). **i**, Results of Pb release test from FPSC module when submerged in a synthetic sweat solution and operated for 24 hours.

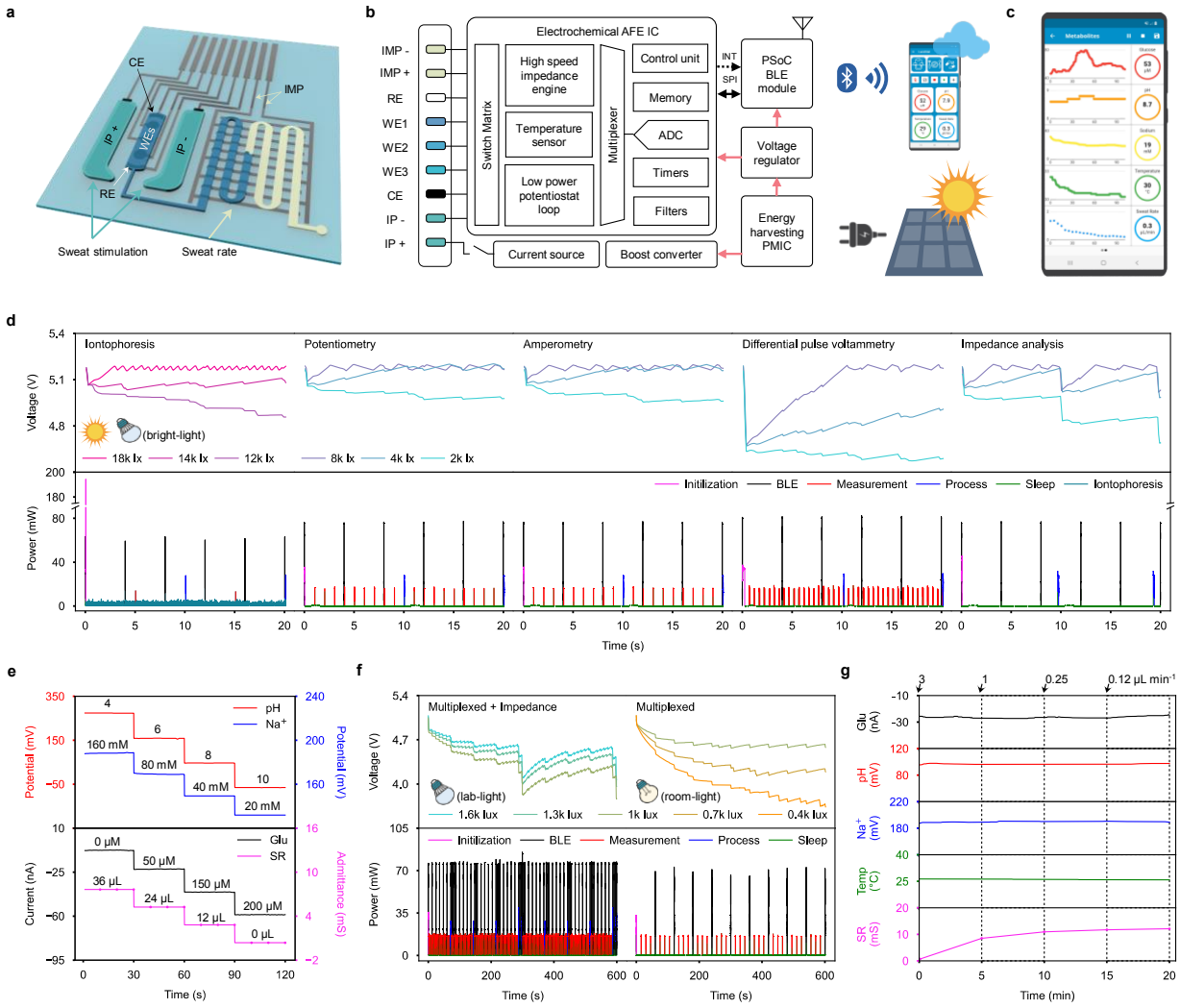

Figure 3 | System design and characterization of the wearable device for energy harvesting and autonomous multimodal biosensing. a, Schematic of the disposable microfluidic sweat patch for sweat induction and sampling. IMP, impedance; CE, counter electrode; WE, working electrode; RE, reference electrode; IP, iontophoresis. **b**, System-level block diagram of the wearable device. **c**, Custom mobile application for the wearable device. ADC, analog to digital converter; AFE IC, analog front end integrated circuit; PsoC, programmable system on chip; INT, interrupt; SPI, serial peripheral interface. **d**, Power consumption profile (bottom) and corresponding capacitor charging-discharging curves (top) of various operation modes under varying light intensities. **e**, Responses of the Na^+, pH, glucose (Glu), and sweat rate (SR) sensors obtained by the wearable device. **f**, Power consumption profile (bottom) and corresponding capacitor charging-discharging curves (top) during multiplexed measurements under indoor lab-light (left) and room-light (right) illumination conditions. **g**, Multiplexed and multimodal sensing response under varying flow rates (0.12–3 µL min^{-1}) and lab-light illumination (1200 lx). Temp, temperature.

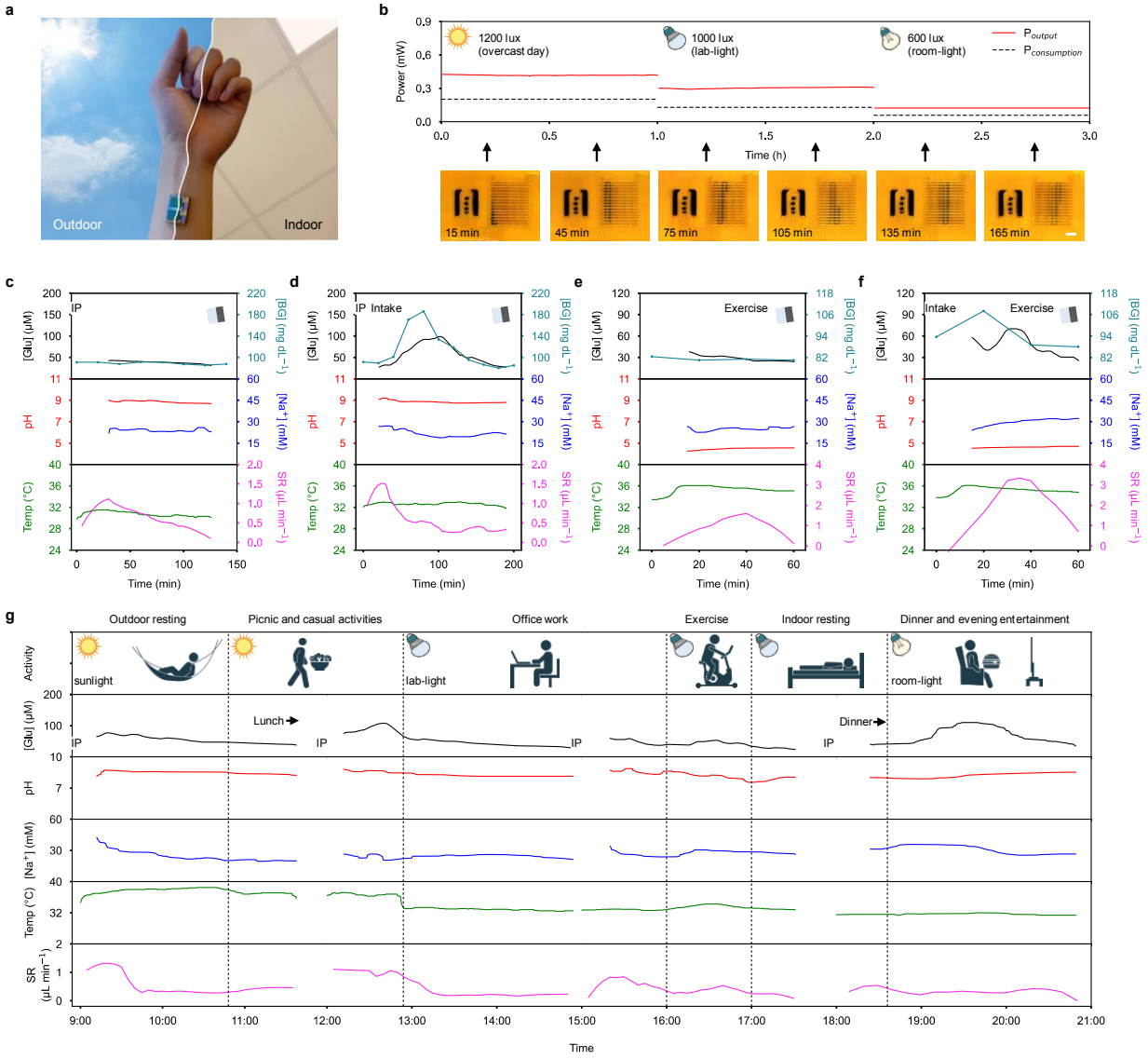

Figure 4 | On-body evaluation of the wearable device for prolonged and cross-activity perspiration analysis. a, Photo of a wearable device worn on-body. **b**, Power output of wearable device's quasi-2D FPSC module and power consumption of the wearable device electronics when performing multiplexed sweat biosensing under various illumination conditions. Inset photos below show the corresponding microfluidic sweat sampling after a single iontophoresis sweat induction event. Scale bar, 3 mm. **c**,**d**, Wearable device-enabled autonomous multiplexed physiological monitoring at a fasting state (**c**) and after a glucose tolerance test (**d**) on a healthy subject under lab-light illumination. IP, iontophoresis. **e**,**f**, Wearable device-enabled multiplexed physiological monitoring during vigorous exercise at a fasting state (**e**) and after a dietary intake

(**f**) under lab-light illumination. **g**, Full-day cross-activity physicochemical monitoring with the wearable device under different light conditions.